Supporting Information

Isotype heterojunction: Tuning the heptazine/triazine phase of crystalline nitrogen-rich C_3N_5 towards multifunctional photocatalytic applications

Sue-Faye Ng,[1,2] Joel Jie Foo,[1,2] Wee-Jun Ong[1,2,3,4,5,*]

[1] *School of Energy and Chemical Engineering, Xiamen University Malaysia, Selangor Darul Ehsan 43900, Malaysia.*

[2] *Center of Excellence for NaNo Energy & Catalysis Technology (CONNECT), Xiamen University Malaysia, Selangor Darul Ehsan 43900, Malaysia.*

[3] *State Key Laboratory of Physical Chemistry of Solid Surfaces, College of Chemistry and Chemical Engineering, Xiamen University, Xiamen 361005, China.*

[4] *Gulei Innovation Institute, Xiamen University, Zhangzhou 363200, China.*

[5] *Shenzhen Research Institute of Xiamen University, Shenzhen 518057, China.*

* Corresponding author

Wee-Jun Ong: Email: weejun.ong@xmu.edu.my

Methodology

1. Materials

Urea (Merck, ≥ 99%), 3-amino-1H-1,2,4-triazole (3AT, Alfa Aesar, 96%), anhydrous lithium chloride (LiCl, Alfa Aesar, 98%), potassium chloride (KCl, Merck, ≥99.5%), sodium sulfate anhydrous (Na_2SO_4, Fisher Scientific, ≥99%) dihydrogen hexachloroplatinate (IV) hexahydrate ($H_2Cl_6Pt{\cdot}6H_2O$, Alfa Aesar), triethanolamine (TEOA, Chemiz), Nafion D-521 dispersion, 5% w/w in water and 1-propanol (Alfa Aesar), isopropyl alcohol (Merck, ≥99.8%), potassium hydrogen phthalate (Fisher Scientific, ≥98.5%), potassium iodide (KI, Merck, ≥99.5%) benzyl alcohol (BA, Alfa Aesar, 99%), and acetonitrile (ACN, Merck, ≥99.9%) were used. All of the materials were of analytical grade and used without further purification. All aqueous solutions were prepared with deionized (DI) water (> 18.2 MΩ cm resistivity).

2. Preparation of pristine C_3N_5 and g-C_3N_4

Pristine C_3N_5 was synthesized through the thermal polymerization of 3AT. Briefly, 2 g of 3AT was placed in a 100 mL crucible, covered and heated to 550 ℃ for 3 h in a muffle furnace with a ramping rate of 10 ℃ min^{-1}. The resulting dark brown powder was ground into a fine powder with a pestle mortar after cooling to room temperature.

Pristine g-C_3N_4 was synthesized through the same route with the substitution of 3AT with 6 g of urea heated to 550 ℃ for a duration of 2 h with a ramping rate of 10 ℃ min^{-1}.

3. Synthesis of crystalline C_3N_5

Crystalline C_3N_5 was synthesized through the molten salt-assisted method with LiCl and KCl. Briefly, 4 g of 3AT, 10.92 g of KCl and 12.96 g of LiCl were ground in a pestle mortar for 10 min. The powder was then transferred to a 100 mL covered crucible with a lid and heated to a certain temperature for 4 h in a muffle furnace with a ramping rate of 12 ℃ min^{-1}. After cooling to room temperature, the powder was washed in DI water at 70 ℃ and separated through filtration then dried at 80 ℃ overnight in an oven. The resulting powder was labelled CC3N5-X, whereby X represents the calcination temperature used (400, 450, 500, 550, and 600 ℃). A representative diagram of this synthesis procedure is depicted in **Figure S1**.

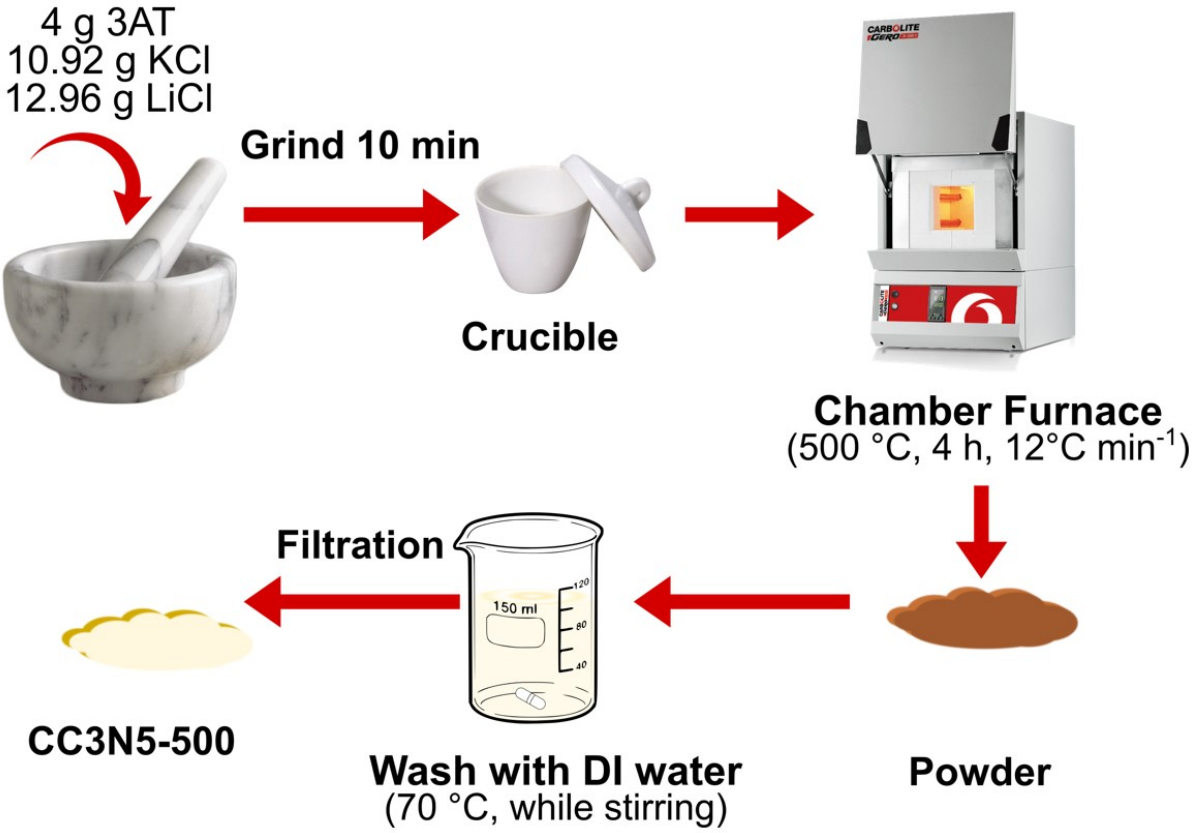

Figure S1. Schematic of crystalline C_3N_5 synthesis prepared at 500 ℃ (CC3N5-500).

4. Characterizations

High resolution transmission electron microscopy (TEM/HRTEM) images were taken by JEOL JEM-2100F microscope equipped with 200 kV field emission analytical electron microscope. Panalytical X'Pert Pro diffractometer with Cu Kα radiation source was acquired to record XRD data at a step size of 0.02° from 5° to 80° (2θ). The Fourier transform infrared spectroscopy (FTIR) spectra were acquired by a PerkinElmer Spectrum Frontier FT-MIR spectrometer, using a standard ATR technique. Each spectrum was generated with a resolution of 8 cm^{-1} from an average of 16 scans between 4000 and 600 cm^{-1}. A JASCOV-770 ST ultraviolet-visible light (UV-Vis) spectrophotometer was used to measure the UV-Vis absorption spectra of the samples ($200 < \lambda < 800$ nm). X-ray photoelectron spectroscopy (XPS) was acquired on Kratos AXIS Ultra DLD spectrometer using Al Kα X-ray radiation of 1486.69 eV with calibration in respect to the C 1s peak at 284.6 eV. Electron paramagnetic resonance (EPR) measurements were performed using a Bruker EMX-10/12 EPR spectrometer. Scanning electron microscopy (SEM) energy dispersive X-ray (EDX) analysis was acquired with Carl Zeiss (GeminiSEM 500).

5. Photocatalytic measurements

Photocatalytic hydrogen evolution reactions were carried out in a quartz glass reactor. 20 mg of photocatalysts were dispersed in a 60 mL aqueous solution containing 10 vol% sacrificial agent (TEOA) as an electron donor and 1 wt% Pt ($H_2PtCl_6 \cdot 6H_2O$). The solution was purged with N_2 gas for 30 min before reaction to remove the residual air. A 300 W Xe lamp (PF300-T8 300W, CEAULIGHT) equipped with a 400 nm cutoff filter was used as a visible light source. The generated H_2 was measured by gas chromatography (Agilent GC 8890, Argon carrier). The reaction was also conducted in the absence of catalyst as a control test, which had no H_2 production, confirming that the hydrogen production was a result of the catalytic reaction between the photocatalyst and water. The photocatalytic HER results were replicated two more times in order to obtain the error bar.

For simultaneous benzyl alcohol oxidation and hydrogen generation, the procedure was similar to the photocatalytic HER setup but replacing the sacrificial agent (TEOA) to benzyl alcohol (3 vol%). Benzaldehyde and its derivatives were quantified by high-performance liquid chromatography (Acquity Arc Waters HPLC system; column: Kinetex 2.6 μm Phenyl-Hexyl 100 Å; injection volume: 10 μL; mobile phase: water/acetonitrile = 60:40; column temperature: 40 °C; flow rate: 1 mL min^{-1}).

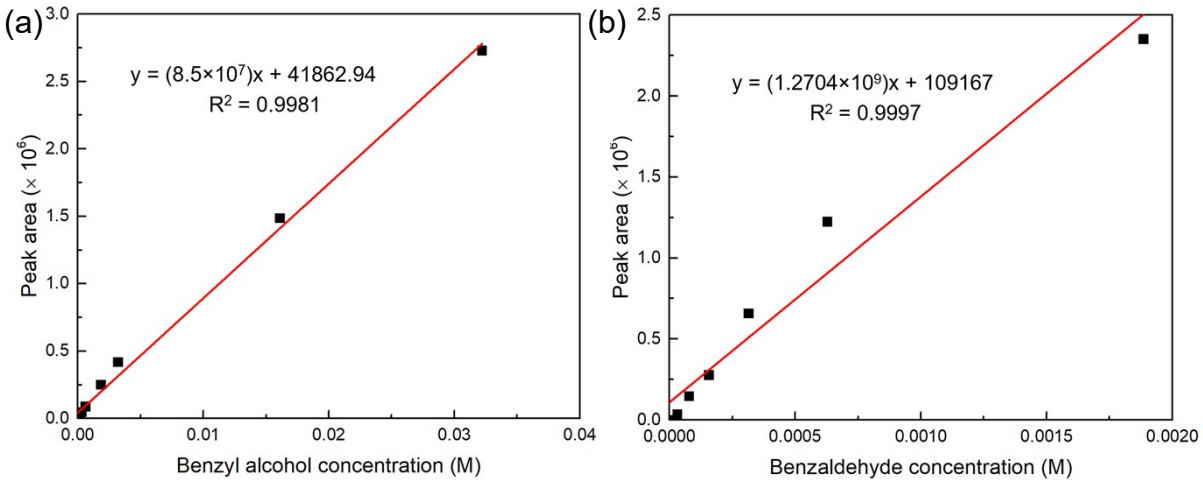

Figure S2. Calibration curve of (a) benzyl alcohol and (b) benzaldehyde concentration against peak area.

For photocatalytic H_2O_2 production, 20 mg catalyst was dispersed into 60 mL aqueous solution containing 10 vol% isopropyl alcohol. The solution was purged with O_2 gas for 30 min before

reaction to remove the residual air. A 300 W Xe lamp (PF300-T8 300W, CEAULIGHT) equipped with a 400 nm cutoff filter was used as a visible light source. The H_2O_2 produced was quantified through an iodometric method. Briefly, 1 mL of suspension was sampled and filtrated to remove the residual photocatalysts. The tested solution was mixed with 1 mL of 0.4 M KI aqueous solution and 1mL of 0.1 M potassium hydrogen phthalate ($C_8H_5KO_4$) aqueous solution. The absorbance was measured by UV−Vis Spectrophotometer (MAPADA UV-1800) at 310 nm after leaving the solution in the dark for 30 min. The calibration curve is shown below.

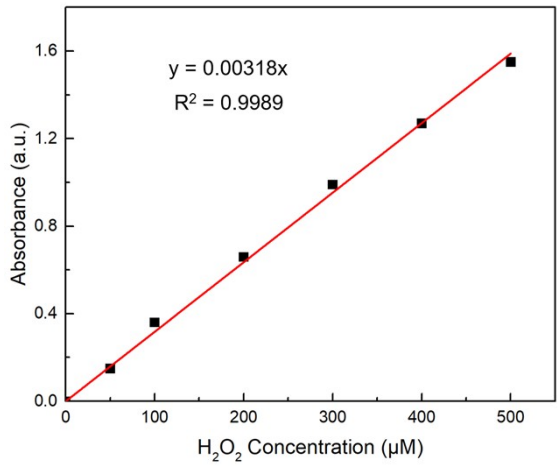

Figure S3. Calibration curve of absorbance and H_2O_2 concentration measured at 310 nm.

Apparent quantum efficiency (AQE) measurements for HER were conducted with different band-pass wavelength irradiations (i.e. 380, 400, 420, 450, and 500 nm). The light intensity was recorded from a spectroradiometer (CEAULIGHT, CEL-NP2000). The AQE value for HER was calculated with the following formula.

$$AQE = \frac{2 \times number\ of\ evolved\ H_2\ molecules}{Number\ of\ incident\ photons} \times 100\%$$

The AQE value for H_2O_2 production was calculated with the following formula.

$$AQE = \frac{2 \times number\ of\ evolved\ H_2O_2\ molecules}{Number\ of\ incident\ photons} \times 100\%$$

The solar-to-hydrogen (STH) conversion efficiency was obtained under simulated sunlight (AM1.5 filter), and was calculated by using the following equation.

$$STH\ (\%) = \frac{R_{H_2} \times \Delta G_{H_2}}{P_{sun} \times S_{irr}} \times 100\%$$

Whereby R_{H_2} denotes the hydrogen evolution rate during the reaction, ΔG_{H_2} is the Gibbs free energy of water decomposition reaction (237.13 kJ mol^{-1}, 25 ℃), P_{sun} is the optical power density of incident sunlight (84.6 mW cm^{-2}) and S_{irr} is the incident area of sunlight (33.18 cm^2).

6. Recyclability

A fused deposition modelling (FDM) 3D printer (3DX Fab Bear MK3S) was used to print out a 5 × 5 cm circle with grid as a substate for the catalyst recyclability test. Clear polycarbonate (PC) filament was used for both the circular grid and the holder. The preparation of substrate ink was as follows: 40 mg of catalyst was added to 2 mL DI water and 0.5 mL Nafion and stirred overnight. The ink was then added dropwise onto the 3D printed substrate and dried in an oven at 60 ℃ for 4 h. The photocatalytic reaction setup was similar to that used during HER experiments in the presence of a water circulating bath at 20 ℃. After each cycle, the substrate was immersed in DI water to wash off any residues from the reaction, and then taken out to be dried in an oven at 60 ℃ before the next cycle.

7. Photoelectrochemical measurements

Photoelectrochemical measurements were performed by an electrochemical workstation (Metrohm Autolab, PGSTAT204) with a standard three-electrode cell, where the prepared sample (working electrode), Pt sheet (counter electrode) and Ag/AgCl (in 3.0 M KCl, reference electrode) were immersed in a 0.1 M Na_2SO_4 solution. The working electrode was prepared with the following procedure. 5 mg of the sample, 40 μL of Nafion and 200 μL of absolute ethanol were stirred overnight. Then, 25 μL of the solution was drop casted onto 1 × 1 cm^2 of a fluorine-doped tin oxide (FTO) glass and dried under ambient temperature. The lifetime of injected electrons (τ) of the photocatalysts were determined via the following expression:

$$\tau = 0.5\pi Fp$$

Whereby Fp represents the inverse minimum frequency.[1]

The transient photocurrent test was conducted with a 300 W Xe lamp equipped with AM1.5 filter at 0.5 V vs. Ag/AgCl.

For the EPR hydroxyl radical test, 10 mg catalyst was added to 1 mL ultrapure water, followed by adding of 45 μL DMPO and ultrasound for 10 min then sealed in a glass tube under argon (Ar) atmosphere for EPR test. The first data point was collected in the dark, and the signal was collected at 10 min of illumination. The EPR superoxide radical test had a similar procedure but with methanol instead of ultrapure water.

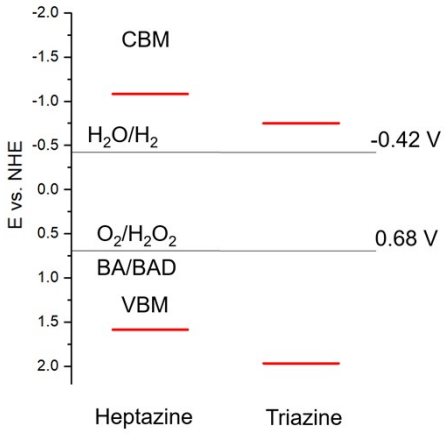

Figure S4. Band structure positions of heptazine and triazine C_3N_5 phase.

Table S1. Element composition of CC3N5-500 as obtained from XPS data.

Element	Content (at%)		
	C_3N_5	CC3N5-500	CC3N5-600
C	22.27	29.80	24.89
N	77.48	54.78	50.96
O	2.55	1.79	2.45
K	-	10.71	0.08
Li	-	2.80	19.19
Cl	-	0.40	1.02

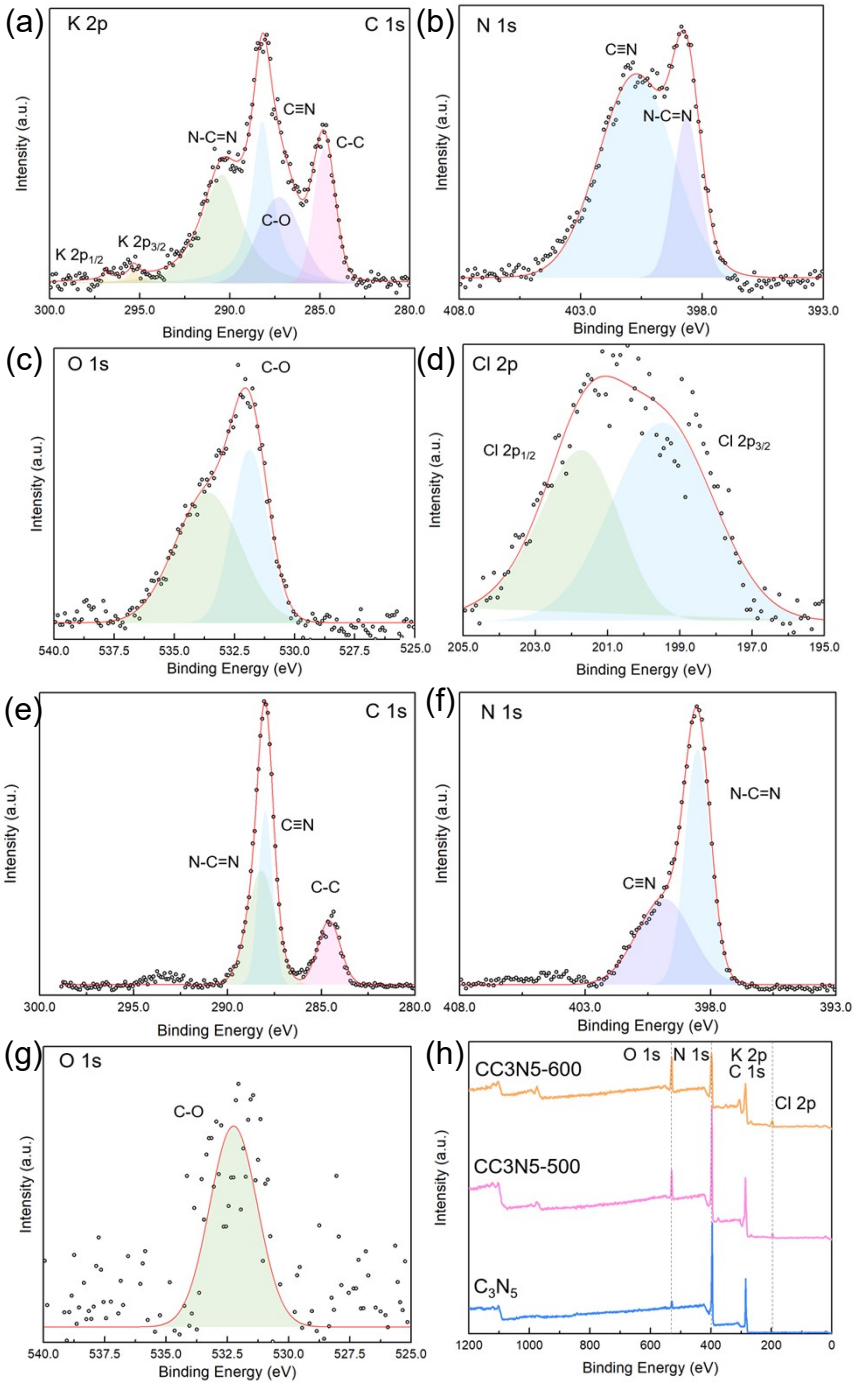

Figure S5. High-resolution XPS spectra of (a) C 1s and K 2p, (b) N 1s, (c) O 1s, and (d) Cl 2p of CC3N5-600. XPS spectra of (e) C 1s, (f) N 1s, (g) O 1s, and (h) survey spectra of pristine C_3N_5, CC3N5-500 and CC3N5-600.

Table S2. Literature comparison of carbon nitride-based photocatalysts for photocatalytic HER.

Photocatalyst	Light Source	HER Generation ($\mu mol\ h^{-1}$)	AQE (%)	Ref.
K doped g-C_3N_4	>420 nm	65.95	-	2
Ni doped g-C_3N_4	>400 nm	26.65	-	3
C_3N_4/C_3N_5	>420 nm	166.5	20.6 (420 nm)	4
NH_2-UiO-66/C_3N_5	>420 nm	19.68	6.78 (420 nm)	5
CdS/C_3N_5	>420 nm	7.86	9.65 (420 nm)	6
Polymeric g-C_3N_4	>420 nm	61.7	-	7
MoP/crystalline g-C_3N_4	>420 nm	265.85	7.2 (420 nm)	8
K-doped crystalline g-C_3N_4	AM1.5	539.00	24.50 (420 nm)	9
B-doped g-C_3N_4	Not Stated	91.97	1.1 (420 nm)	10
Porous g-C_3N_4	>410 nm	85.47	7.5 (430 nm)	11
CC3N5-500	>400 nm	359.97	12.86 (420 nm)	This work
CC3N5-500	AM1.5	558.54	-	This work

Table S3. Apparent quantum efficiency (AQE) calculation data for the optimal CC3N5-500.

Wavelength	380	400	420	450	500
H_2 evolution ($\mu mol\ h^{-1}$)	107.03	145.62	150.97	15.35	0
Light intensity/area ($mWcm^{-2}$)	8.29	31.8	63.2	24.8	87.8
AQE (%)	76.82	25.89	12.86	3.11	0

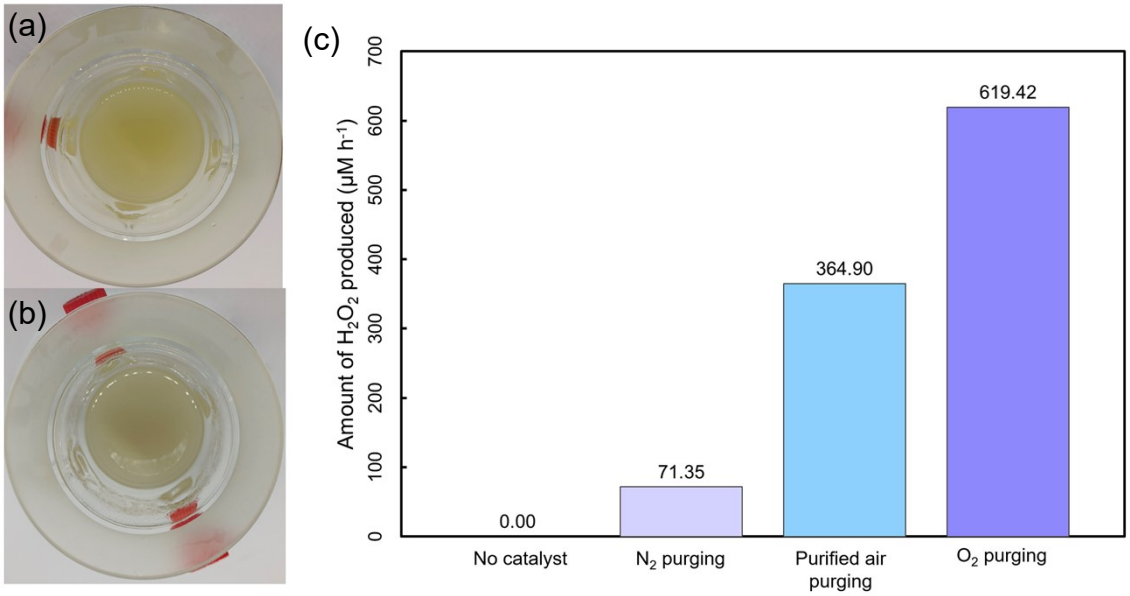

Figure S6. Picture of CC3N5-500 (a) before and (b) after simultaneous HER and benzyl alcohol photocatalytic oxidation. (c) Control tests for photocatalytic H_2O_2 production on CC3N5-550.

Table S4. Literature comparison of carbon nitride-based photocatalysts for simultaneous photocatalytic HER and BA oxidation.

Photocatalyst	Light Source	HER Generation (μmol h^{-1})	BAD Generation (μmol h^{-1})	Ref.
N-defect g-C_3N_4	>420 nm	9.80	9.91	[12]
Crystalline g-C_3N_4	>420 nm	49.06	44.16	[13]
S-doped g-C_3N_4	>420 nm	3.76	3.87	[14]
Ru-doped crystalline g-C_3N_4	$320 \leq \lambda \leq 850$ nm	57.5	43.2	[15]
Carbon modified g-C_3N_4	>420 nm	2.88	2.31	[16]
W-doped g-C_3N_4	>420 nm	2.99	3.05	[17]
Ni doped black phosphorus-g-C_3N_4	>420 nm	0.928	0.939	[18]
CC3N5-500	>400 nm	85.91	1490.36	This work

Table S5. Literature comparison of carbon nitride-based photocatalysts for H_2O_2 production.

Photocatalyst	Light Source	H_2O_2 Generation ($\mu mol\ L^{-1}\ h^{-1}$)	AQE (%)	Ref.
K/Na doped N-defect g-C_3N_4	>420 nm	25.5	30.7 (429 nm)	19
N-defect g-C_3N_4	>420 nm	46.85	3.8 (420 nm)	20
Porous g-C_3N_4 nanotube	>420 nm	93.83	-	21
B/O doped defect g-C_3N_4	>420 nm	24.8	-	22
Methyl viologen ionized g-C_3N_4	>420 nm	114.2	44.5 (420 nm)	23
B-doped g-C_3N_4	>420 nm	7.97	-	24
Ultrathin g-C_3N_4	>400 nm	13.3	4.2 (420 nm)	25
WO_3/g-C_3N_4	>400 nm	161	-	26
CC3N5-550	>400 nm	619.42	20.90 (400 nm) 9.49 (420 nm)	This work

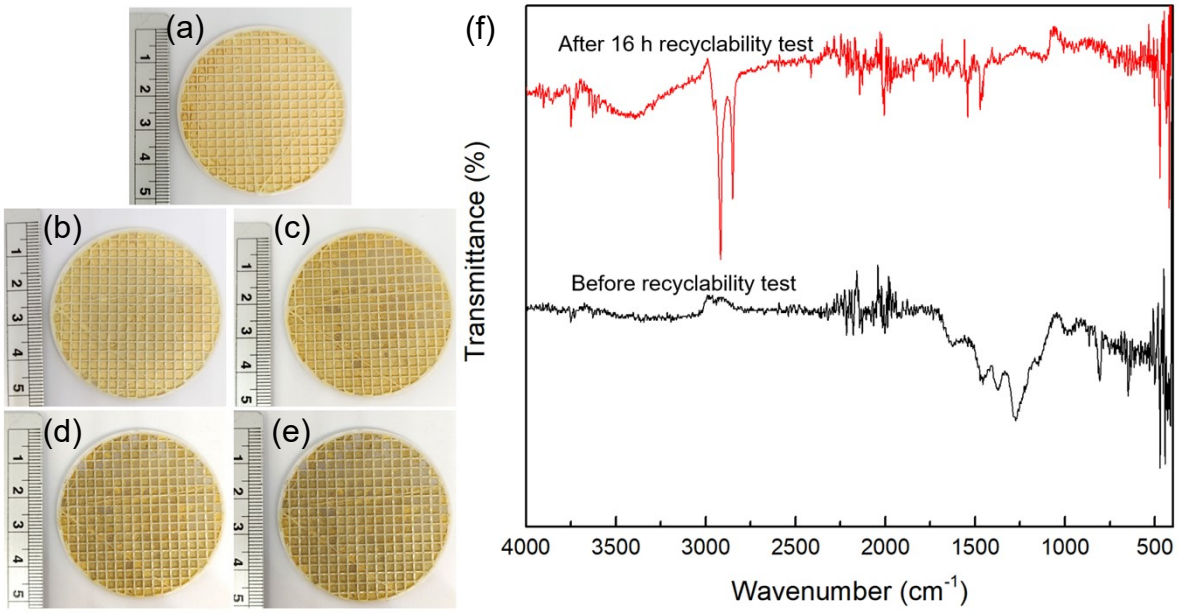

Figure S7. Pictures of 3D printed substrate loaded with CC3N5-500 catalyst (a) before reaction, after (b) 1 cycle, (c) 2 cycles, (d) 3 cycles, and (e) 4 cycles. (f) FTIR measurements for CC3N5-500 photocatalysts before and after the recyclability test.

Table S6. Lifetime of injected electrons (τ), inverse minimum frequency (Fp), ohmic resistance (Rp.S), and charge transfer resistance (Rp.R) calculated from the EIS spectra of carbon nitride catalysts.

Sample	τ (ms)	Fp (Hz)	Rp.R (MΩ·cm^{-2})
g-C_3N_4	1265.14	0.13	1.10×10^6
C_3N_5	399.89	0.40	6.58
CC3N5-400	12642.38	0.01	1.10×10^6
CC3N5-450	50.37	3.16	0.287
CC3N5-500	50.33	3.16	0.0634
CC3N5-550	126.42	1.26	0.655
CC3N5-600	159.15	1.00	1.61

.

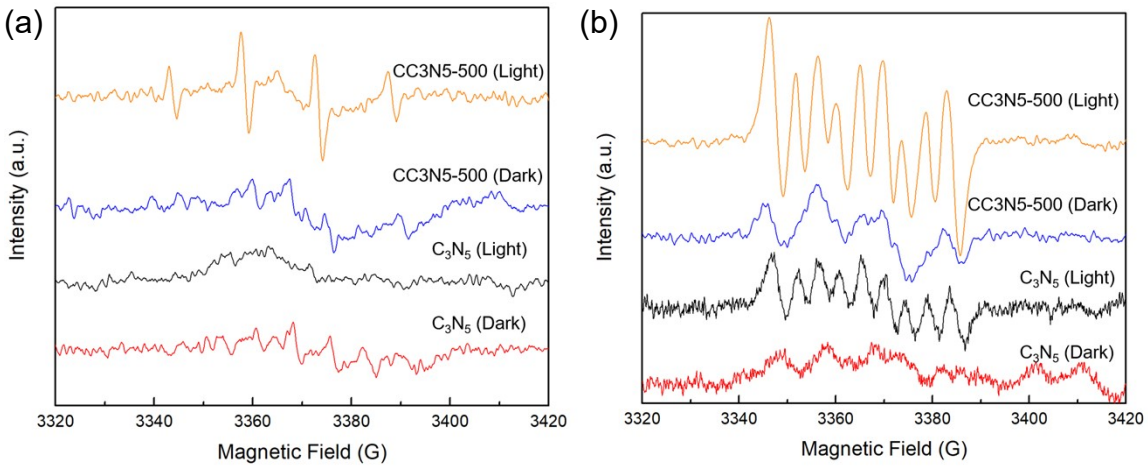

Figure S8. EPR spectra of (a) DMPO-•OH and (b) DMPO-•O_2^- compounds over pristine C_3N_5 and CC3N5-500 in the dark and under light illumination for 10 min.

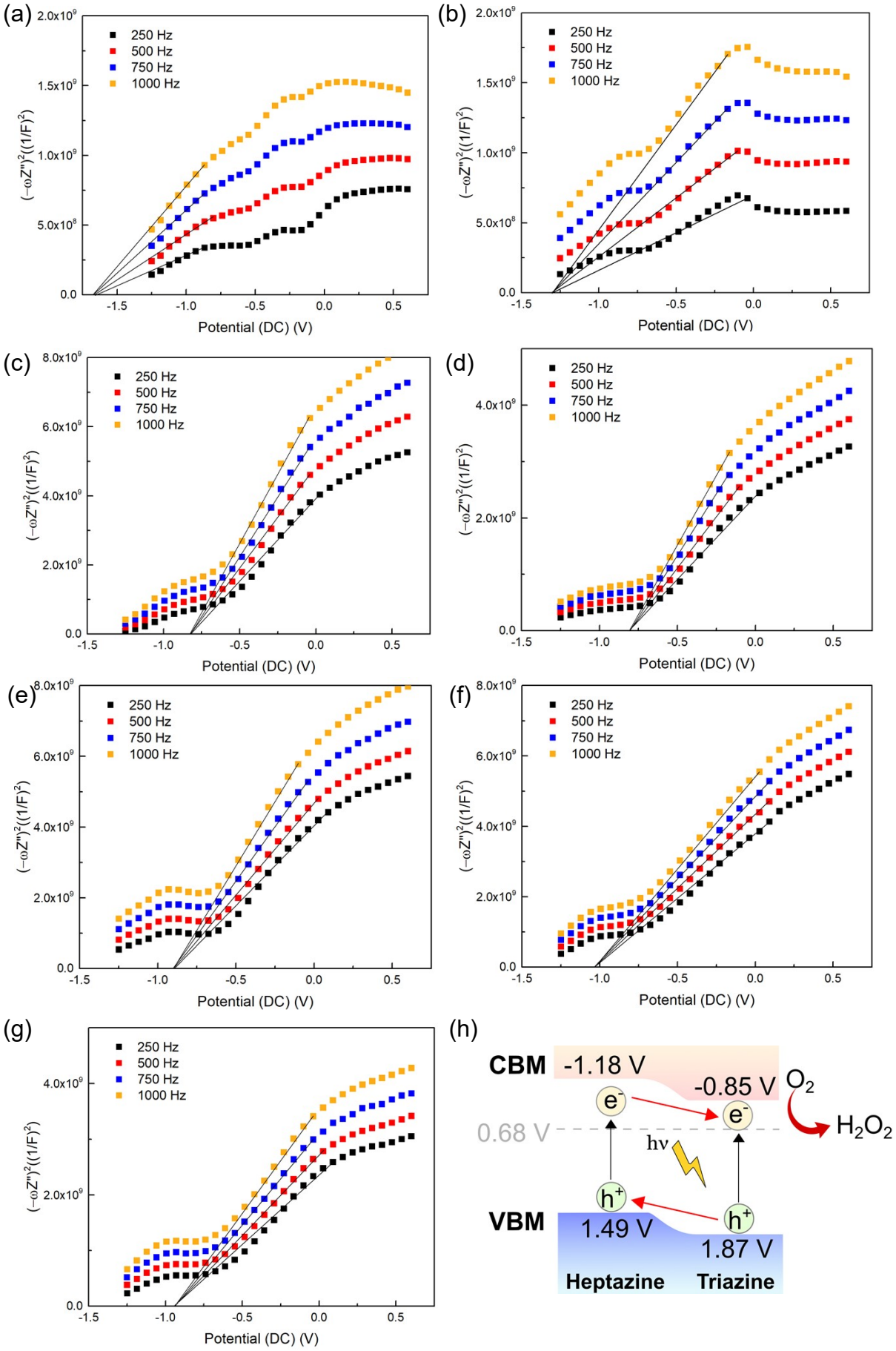
(a)
(b)
(c)
(d)
(e)
(f)
(g)
250 Hz
500 Hz
750 Hz
1000 Hz
Potential (DC) (V)
(−ωZ'')²((1/F)²)
(h)
CBM
-1.18 V
-0.85 V
O2
H2O2
0.68 V
hν
VBM
1.49 V
1.87 V
Heptazine
Triazine

Figure S9. Mott Schottky plots for (a) g-C_3N_4, (b) C_3N_5, (c) CC3N5-400, (d) CC3N5-450, (e) CC3N5-500, (f) CC3N5-550, and (g) CC3N5-600. (h) Band position of the CC3N5-500 catalyst.

Table S7. CB and VB positions of carbon nitride samples.

Sample	CB (eV vs. NHE)	VB (eV vs. NHE)
g-C_3N_4	-1.583	1.397
C_3N_5	-1.183	1.487
CC3N5-400	-0.713	2.067
CC3N5-450	-0.71	2.08
CC3N5-500	-0.793	1.857
CC3N5-550	-0.933	1.707
CC3N5-600	-0.853	1.867

References

1. C. Liu, H. Huang, X. Du, T. Zhang, N. Tian, Y. Guo and Y. Zhang, *J. Phys. Chem. C*, 2015, **119**, 17156-17165.
2. X. Chang, H. Fan, S. Zhu, L. Lei, X. Wu, C. Feng, W. Wang and L. Ma, *Ceram. Int.*, 2023, **49**, 6729-6738.
3. Y.-C. Huang, Y. Li, K. T. Arul, T. Ohigashi, T. T. T. Nga, Y.-R. Lu, C.-L. Chen, J.-L. Chen, S. Shen, W.-F. Pong, C.-L. Dong and W.-C. Chou, *ACS Sustain Chem. Eng.*, 2023, **11**, 5390-5399.
4. N. Su, S. Cheng, P. Zhang, H. Dong, Y. Fang, X. Zhou, Y. Wang and C. Li, *International Journal of Hydrogen Energy*, 2022, **47**, 41010-41020.
5. B. Wu, T. Sun, N. Liu, L. Lu, R. Zhang, W. Shi and P. Cheng, *ACS Appl. Mater. Interfaces*, 2022, **14**, 26742-26751.
6. X. Wang, K. Wu, W. Cao, K. Rui, W. Wang, R. Zhu, J. Zhu and Z. Yan, *Adv. Mater. Interfaces*, 2023, **10**, 2201627.
7. X. Lin, H. Du, D. Jiang, P. Zhang, Z. Yu, H. Bi and Y. Yuan, *J. Energy Chem.*, 2022, **65**, 541-547.
8. L. Cao, Y. Shi, Z. Chen, Y. Tian, L. Chen, F. Guo and W. Shi, *Mater. Today Comm.*, 2022, **33**, 104354.
9. S. Yang, H. Zhang, J. Wang, J. Xiang, Z. Fu, Y. Wang, Z. Li, H. Xie, S. Tang and Y. Li, *Appl. Surf. Sci.*, 2023, **616**, 156523.
10. W. Dai, R. Wang, Z. Chen, S. Deng, C. Huang, W. Luo and H. Chen, *J. Mater. Chem. A*, 2023, **11**, 7584-7595.
11. S. Mondal, G. Mark, L. Abisdris, J. Li, T. Shmila, J. Tzadikov, M. Volokh, L. Xing and M. Shalom, *Mater. Horiz.*, 2023, **10**, 1363-1372.
12. X. Liu, Q. Zhang, Z. Cui, F. Ma, Y. Guo, Z. Wang, Y. Liu, Z. Zheng, H. Cheng, Y. Dai, B. Huang and P. Wang, *International Journal of Hydrogen Energy*, 2022, **47**, 18738-18747.
13. T. Huo, Q. Deng, F. Yu, G. Wang, Y. Xia, H. Li and W. Hou, *ACS Appl. Mater. Interfaces*, 2022, **14**, 13419-13430.
14. F. Zhang, J. Li, H. Wang, Y. Li, Y. Liu, Q. Qian, X. Jin, X. Wang, J. Zhang and G. Zhang, *Appl. Catal., B*, 2020, **269**, 118772.

15. Q. Yang, T. Wang, Z. Zheng, B. Xing, C. Li and B. Li, *Appl. Catal., B*, 2022, **315**, 121575.
16. H. Wang, J. Zhang, X. Jin, X. Wang, F. Zhang, J. Xue, Y. Li, J. Li and G. Zhang, *J. Mater. Chem. A*, 2021, **9**, 7143-7149.
17. F. Zhang, J. Zhang, H. Wang, J. Li, H. Liu, X. Jin, X. Wang and G. Zhang, *Chem. Eng. J.*, 2021, **424**, 130004.
18. M. Wen, N. Yang, J. Wang, D. Liu, W. Zhang, S. Bian, H. Huang, X. He, X. Wang, S. Ramakrishna, P. K. Chu, S. Yang and X.-F. Yu, *ACS Appl. Mater. Interfaces*, 2021, **13**, 50988-50995.
19. S. Wu, H. Yu, S. Chen and X. Quan, *ACS Catal.*, 2020, **10**, 14380-14389.
20. Y. Zheng, Y. Luo, Q. Ruan, S. Wang, J. Yu, X. Guo, W. Zhang, H. Xie, Z. Zhang and Y. Huang, *Appl. Catal., B*, 2022, **311**, 121372.
21. Y. Song, C. Zhou, Z. Zheng, P. Sun, Y. She, F. Huang, Z. Mo, J. Yuan, H. Li and H. Xu, *J. Alloys Compd.*, 2023, **934**, 167901.
22. Q. You, C. Zhang, M. Cao, B. Wang, J. Huang, Y. Wang, S. Deng and G. Yu, *Appl. Catal., B*, 2023, **321**, 121941.
23. Y. Zhao, J. Gao, Z. Yang, L. Li, J. Cui, P. Zhang, C. Hu, C. Diao and W. Choi, *ACS Catal.*, 2023, **13**, 2790-2801.
24. B. P. Mishra, L. Acharya and K. Parida, *Catal. Sci. Technol.*, 2023, **13**, 1448-1458.
25. J. Hu, P. Zhang, T. Yang, Y. Cai, J. Qu and X. Yang, *Appl. Surf. Sci.*, 2022, **576**, 151841.
26. M. Jourshabani, S. H. Yun, M. Razi Asrami and B. K. Lee, *Chem. Eng. J.*, 2022, **427**, 131710.